Forecasting Operational Parameters of a Solar Space Heating System using a Novel Multistage Artificial Neural Network

Farnaz Jamadi *
Department of Physics,
Sirjan University of Technology, Iran
E-mail: f_jamadi@sirjantech.ac.ir
*Corresponding author

Behnam Jamali
Department of Mechanical Engineering,
Sirjan University of Technology, Sirjan, Iran
E-mail: jamalibrocket@gmail.com

Received: 27 November 2017, Revised: 23 February 2018, Accepted: 29 April 2018

Abstract: In this study, several operational parameters of a solar energy system are predicted through using a multistage ANN model. To achieve the best design of this model, three different back-propagation learning algorithms, i.e. Levenberg-Marquardt (LM), Pola-Riber Conjugate Gradient (CGP) and the Scaled Conjugate Gradient (SCG) are utilized. Further, to validate the ANN results, some experimental tests have been done in winter 2016 on a solar space heating system (SSHS) equipped with a parabolic trough collector (PTC). In the proposed model, ANN comprises three consecutive stages, while the outputs of each one are considered to be the inputs of the next. Results show that the maximum error rate in Stages 1, 2, and 3 has occurred in the LM algorithm with respectively 10, 6, and 10 neurons. Moreover, the best obtained determination coefficient of all stages belongs to the total system efficiency and has the value 0.999934 for LM-10. As a result, the multistage ANN model can simply forecast operational parameters of the solar energy systems with high accuracy.

Keywords: Multistage neural network, Operational parameters, Solar space heating system, Total system efficiency

Reference Farnaz Jamadi and Behnam Jamadi, "Forecasting Operational Parameters of a Solar Space Heating System, Using a Novel Multistage Artificial Neural Network", Int J of Advanced Design and Manufacturing Technology, Vol. 11/No. 2, 2018, pp. 75-84.

Biographical notes: F. Jamadi received her BSc and MSc degrees in Nuclear Physics from the Shahid Bahonar University of Kerman, Kerman, Iran. She is currently instructor of Physics at Sirjan University of Technology, Sirjan, Iran. Her research activities are radon and solar energy. She has 5 scientific and research publications. **B. Jamali** received his BSc in Mechanical engineering from the Sirjan University of Technology, Sirjan, Iran. His research activities are Artificial neural network and solar energy. He has 2 scientific and research publications.

1 INTRODUCTION

In the past decades, worldwide energy crisis and environmental problems such as ozone destruction have caused the governments' move to replace nearly-ending fossil fuels with renewable energies. On the other hand, Sunny hours in Iran average 2054 h yearly [1]. Therefore, application of solar energy as an environmentally friendly energy would be very effective. Solar collectors have domestic and industrial applications such as electricity generation systems, solar water heater systems and solar space heating and cooling systems. As 40% of the world's total energy consumption is related to building applications [2], utilizing domestic solar energy systems would bring many economic advantages. Determining the performance of solar heating systems experimentally, needs expensive devices, long time and lots of calculations. Thus, in order to save time and cost, the solar energy system's performance should be predicted and evaluated prior to being manufactured and set up in an especial area. To this end, prediction through ANN constitutes a common technique in building energy applications, as many researchers have used single stage ANN with different algorithms to forecast the performance of energy systems.

The heat consumption of a university with various ANN models and an adaptive neuro-fuzzy inference system was predicted by Jovanovic et al., who designed three different models of inputs for each ANN model type. Finally, three models were suggested to predict thermal energy consumption [3]. In order to forecast energy consumption in a building category through ANNs, a new method was presented by Ascione et al. [4]. The performance of building heating load was evaluated, using a dynamic ANN, by Sholahudin and Han. An apartment building was simulated through the Energy-plus software, and different combinations of input parameters were studied so as to forecast the heating load using Taguchi method. This method can well decrease the number of ANN input parameters [5]. Deb et al. have accomplished an energy analysis of industrial buildings to calculate the cooling load energy. To predict {the} energy consumption of building for the next days, they have utilized five previous days' data [6]. In addition, Argirioua et al. designed a controller for space heating systems in solar buildings using a feed-forward back-propagation ANN. They employed the environmental data as ANN inputs to study model capabilities. Consequently, the use of a common controller results in energy savings of about 15% in European weather conditions [7]. Kalogirou studied applications of ANN and genetic algorithms in detail for the simulation, modelling, and forecasting the solar energy system performance [8]. Furthermore, Boukelia et al. have optimized a solar parabolic trough collector using ANN with three algorithms for the economical purposes. The obtained parameters showed that the LM algorithm, with 38 neurons in a hidden layer, is the best model of ANN to predict the annual power generation [9]. In order to achieve maximum solar energy for domestic space heating and water heater, Hirvonen et al. have carried out an optimization by applying a multi-objective neural network [10]. Yaïci et al. investigated the effect of the number of input variables (varying from seven to nine) on the precision of the ANN method. Although they concluded that the accuracy of the ANN model would decrease with fewer parameters, their models (with 20 neurons and eight outputs) were able to predict the performance of the solar energy system well [11]. Investigation on heat absorption and loss rates in solar collectors have been done by Liu et al. through applying an ANN model which portrayed high accuracy [12]. In spite of many researches in the previous literature on the application of ANNs in assessing the energy performance of buildings, the parameters were not predicted simultaneously. In fact, none of the studies succeeded to forecast all operational parameters of SSHS by using a multi-stage ANN; they only applied single-stage ANN models. In some researches of course, multi-stage ANN was applied to predict solar radiation in a few cities [13], [14]. However, there are few studies that exploit the multi-stage ANN to forecast the SSHS performance.

In this study, first a space heating system has been designed and set up in Kerman province (with high radiation potential). To augment the system performance, the PTC is applied to the solar heating system. Since parabolic solar collectors have the ability of tracking sun, they seem to be stronger than flat plate collectors. To forecast operational parameters, a multistage ANN model is used, consisting of three single-stage ANNs. The model can simultaneously predict all parameters related to the SSHS such as useful energy of the collector, heat exchanger, radiator, delivered heat to the room, collector efficiency, heat exchanger efficiency, and the total efficiency. Comparison between the multistage ANN results and the experimental data show that multistage ANN is a reliable and fast method to calculate operational parameters.

2 DESCRIPTION OF THE ANN MODEL

ANN is a strong technique for analysing complicated engineering problems. ANN was designed to mirror the biological structure of the human brain. The type and size of ANN depends on the complication of the studied problem and the relations between neurons. As neurons can learn and communicate with different types of data, they are first trained in this method. Then, they will try to find logical relations between input and output data. Properties of ANN are determined by certain factors:

(1) weight coefficients that determine each input's contribution to the output result, (2) hidden layer size; and (3) the type of algorithm that trains the ANN model. There are different algorithms to find relations between inputs and outputs, the most common of which is back-propagation, and the most applicable to the energy field are LM, CGP, and SCG. The performance of ANN models is evaluated by a statistical analysis, Root mean square error (RMSE), mean percentage error (MPE), and the determination coefficient (R^2) are defined as in ''Eqs. (1), (2) and (3)'' [15].

$$RMSE=\sqrt{\frac{1}{n}\sum_{i=1}^{n}(y_{out,i}-E_i/y_{out,i})^2} \quad (1)$$

$$MPE=\frac{1}{n}\sum_{i=1}^{n}[(y_i-E_i)/\left|E_{max}-E_{min}\right|]\times 0.100 \quad (2)$$

$$R^2=\left[\sum_{i=1}^{n}(y_i-\overline{y_i})(E_i-\overline{E_i})/\sqrt{\sum_{i=1}^{n}(y_i-\overline{y_i})^2\sum_{i=1}^{n}(E_i-\overline{E_i})^2}\right]^2 \quad (3)$$

y_i is the output value, $\overline{y_i}$ denotes the average output value; E_i represents the experimental value, E_i refers to the average experimental value; and n is the total number of values. If there is only one system parameter to be estimated by ANN, and there are few inputs for validation, the single stage ANN can predict the target well. Nevertheless, if there are many types of data and several target parameters, the single stage ANN would have insufficient efficiency. The best advantage of multistage ANN compared to the single stage is the ability of sharing operational parameters for evaluating total efficiency. Multistage ANN can also predict important system parameters simultaneously.

3 MATERIALS AND METHODS

3.1. Description of Solar Heating System

Here, the SSHS is used to heat a room of 10 m^2 area. As illustrated in ''Fig. 1,'' original components of the SSHS are: a PTC, a counter-flow heat exchanger, an energy storage tank (17 L), and a radiator. The SSHS has two separate cycles: oil and water. The oil is pumped from its tank to the PTC's absorber tube, where it absorbs thermal energy from solar radiation, and then enters the heat exchanger. Inside the heat exchanger, water coming from the storage tank receives heat from the hot oil, and again returns to the tank. Finally, warm water goes to the radiator and delivers heat to the room.

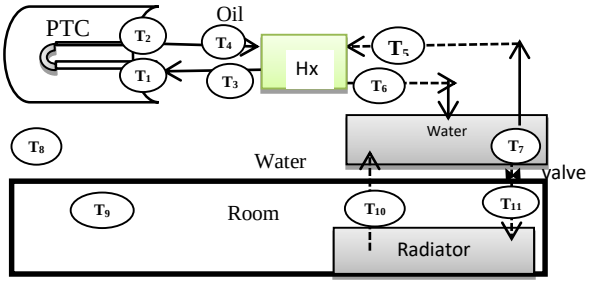

Fig. 1 Schematic of solar heating system.

3.2. Experimental Method

Experiments with SSHS were carried out from 9 AM to 3 PM on February 28, 2016 in Sirjan (city) at location 29° 28′ N, 55° 34′ E, and altitude 1743m. The heating systems were installed on the roof of the building. Note that, to evaluate the SSHS performance, the heat transfer fluid temperature, solar radiation, and the ambient temperature were measured. Furthermore, the axis of PTC was set in north-south direction, in order to receive the maximum solar energy. The sensor locations for measuring these temperatures are shown in ''Fig. 1.'' Two four-channel data loggers were used to record the temperatures of the collector and heat exchanger fluids. The radiator temperature in turn was measured using a PT100 RTD class sensor. Lastly, the solar radiation was assessed through a pyranometer. The data collection was done every 15 minutes, a time interval that is necessary to reach the steady state conditions for a solar energy system [16]. Characteristics of the measurement devices are given in ''Table 1''.

Table 1 Characteristics of measurement devices

Instrument	Accuracy	Range	Model
Pyranometer	±1Wm^{-2}	Up 2000Wm^{-2}	TES-1333
Temperature meter	±0.05% ±0.2°C	-190°C +790°C	TES-1317
Temperature meter	±0.05%±1 °C	-148°C +1370°C	TES-1384

4 THERMAL ANALYSIS OF SOLAR HEATING SYSTEM

In space heating process, each system component has a key role in determining the total efficiency of the system. Therefore, in addition to collector, the heat exchanger, the energy storage tank, and the radiator should be considered heat-transfer blocks. The useful energy rate of the collector can be calculated by ''Eq. 4.''

$$\dot{Q}_c=\dot{m}_f C_f (T_2-T_1) \quad (4)$$

Besides, the thermal efficiency of the collector is given as follows [17]:

$$\eta_c = \dot{m}_f C_f (T_2 - T_1)/(IA_c) \quad (5)$$

Where A_c and I denote the collector surface area and the solar radiation, respectively. The collector's useful energy is the sum of the absorbed energy over time [17]:

$$Q_c = \int_{t_1}^{t_2} \dot{Q}_c dt \quad (6)$$

The received energy of the storage tank is given as:

$$Q_w = m_w C_w \Delta T_w \quad (7)$$

Where m_w, and T_w are respectively: mass, heat capacity, and temperature of the tank water. Delivered thermal energy to the room would be defined as:

$$Q_R = m_w C_w (T_{11} - T_{10}) \quad (8)$$

Where T_{10} and T_{11} are, respectively, the inlet and outlet water temperatures of the radiator. The maximum heat that cold water can receive from the hot oil is calculated as:

$$Q_{w,H} = m_w C_w (T_6 - T_5) \quad (9)$$

While T_5 and T_6 respectively represent the inlet and outlet water temperatures of heat exchanger, where the hot oil transfers thermal energy, as in ''Eq. 10,'' to the cold water:

$$Q_{o,H} = m_o C_o (T_3 - T_4) \quad (10)$$

While, T_4 and T_3 refer, respectively, to the inlet and outlet oil temperatures of heat exchanger. The efficiency coefficient of the heat exchanger is defined as in ''Eq. 11'' [17]:

$$\eta_H = Q_{o,H}/[m_o C_o (T_4 - T_5)] \quad (11)$$

After all, the total efficiency of SSHS would be:

$$\eta_t = Q_R/(IA_c) \quad (4)$$

5 RESULTS AND DISCUSSION

5.1. Experimental Investigations

Inlet and outlet fluid temperatures of collector and heat exchanger, along with the storage tank temperature, the ambient temperature and the solar radiation were all measured on February 26, 2016. As illustrated in ''Fig. 2'', the average value of solar radiation is 690 Wm^{-2}, decreasing in the afternoon hours. It was a sunny day and the maximum solar radiation of this day was 780 Wm^{-2}.

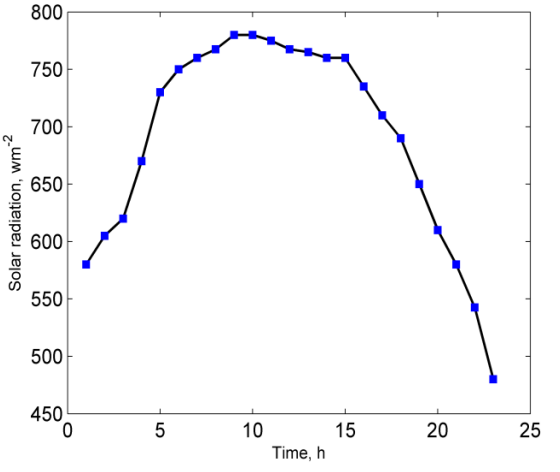

Fig. 2 Solar radiation values versus time.

Figure 3 shows the outlet and inlet oil temperatures of the collector along with those of the heat exchanger. The maximum oil temperatures at the collector and the heat exchanger, are respectively 120°C and 112°C at 12:00. They increased with the rise of solar radiation up to 12:00 noon, and were decreasing after that.

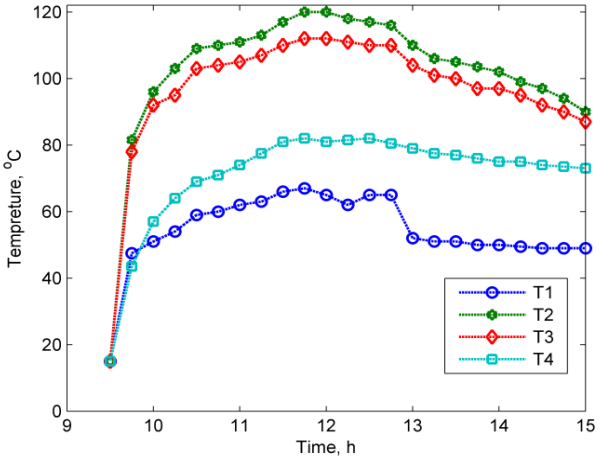

Fig. 3 Temperatures of the collector and heat exchanger fluids.

Figure 4 portrays room and ambient temperatures during the time. Room temperature increases from 16.5°C to 17.5°C at 11:45 pm, then, rapidly rises to 21.9°C at 12:30 pm. The reason lies in the storage tank's valve being closed up to 11:45, and being open afterwards, when the space heating system started to deliver thermal energy to the room. Thereafter, temperature maintains a nearly constant 22°C.

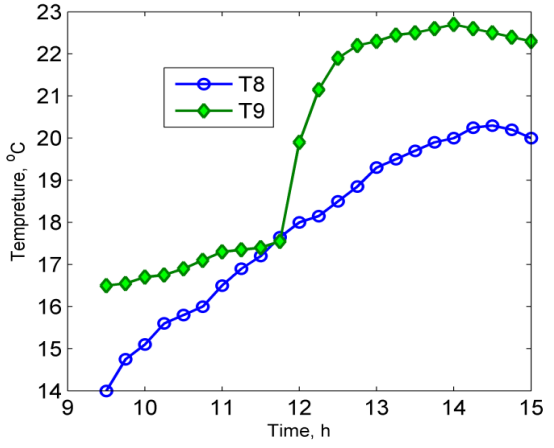

Fig. 4 Room and ambient temperatures versus time.

5.2. ANN Results

The present study uses a multistage ANN model, comprising three stages, for predicting the operational parameters of the SSHS. Each stage, in turn, is a single-stage ANN. Levenberg-Marquardt, Pola-Riber Conjugate Gradient, and the Scaled Conjugate Gradient algorithms are applied to all three stages. In Stage 1, six parameters constitute ANN inputs, i.e. ambient temperature, water temperature of the storage tank, outlet oil temperature of the collector, outlet oil temperature of the heat exchanger, water temperature of the heat exchanger, and the solar radiation.

Table 2 RMSE and MPE of collector's useful energy for all data

Q_C				All data
Algorithm	hl	R_t^2	MPE	RMSE
LM	4	0.990682	0.016878	0.028146
LM	5	0.978132	0.026147	0.045182
LM	6	0.982933	0.026653	0.034954
LM	8	0.978044	0.025563	0.039592
LM	9	0.967583	0.030795	0.051617
LM	10	0.99519	0.008011	0.019779
CGP	3	0.975158	0.027242	0.043552
CGP	5	0.983787	0.023658	0.0346
CGP	7	0.966363	0.040704	0.0499
SCG	3	0.979362	0.028093	0.03949
SCG	7	0.980447	0.026666	0.041562
SCG	9	0.965782	0.03869	0.05204

Accordingly, the useful energy of the collector, energy transferred by the heat exchanger oil, energy obtained by the heat exchanger water, and the delivered energy to the room are ANN outputs. Figure 5 shows the structure of the three-stage neural network.

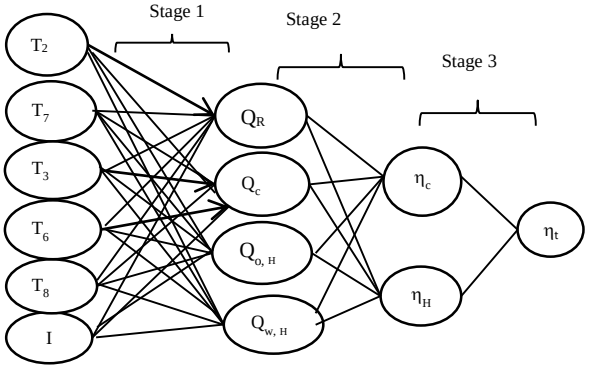

Fig. 5 Structure of the three-stages neural network.

RMSE and MPE of collector's useful energy are brought into Table 2 for all data. Maximum and minimum R^2, MPE and RMSE values have been emboldened in all tables. Neural networks with LM, SCG and CGP are trained for 3, up to 10, the number of hidden layers are shown in the following Tables.

According to Table 2, Maximum R^2s for train and all data are respectively 0.999996 & 0.99519, with RMSEs 0.000601 & 0.019779, and MPEs 0.00037 & 0.008011. Figure 6 shows the predicted and experimental useful energy of the collector. There is a good agreement between the two values for LM 10. The useful energy of the collector is accompanied by solar radiation increments, increasing from morning up to noon. It has its maximum value at 1:00 pm; thereafter decreasing in the afternoon.

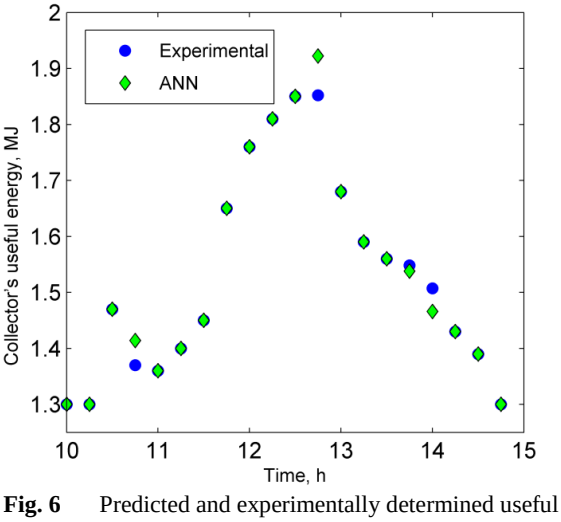

Fig. 6 Predicted and experimentally determined useful energy of the collector, versus time.

Statistical values of oil energy of the heat exchanger are presented in Table 3. Maximum R^2s for train and all data are respectively 0.999382 & 0.934115, with RMSEs 0.005523 & 0.037041, and MPEs 0.003354 & 0.037041.

Table 3 RMSE and MPE for train data for the heat exchanger's oil energy

$Q_{o,H}$				Train data
Algorithms	hl	R_{tr}^2	MPE	RMSE
LM	4	0.992987	0.014154	0.017408
LM	5	0.994995	0.012382	0.015343
LM	6	0.996004	0.011437	0.013866
LM	7	0.99556	0.017204	0.02154
LM	8	0.992202	0.03866	0.040865
LM	9	0.991368	0.021845	0.031956
LM	10	0.999382	0.003354	0.005523
CGP	3	0.990327	0.020382	0.023246
CGP	5	0.991228	0.013668	0.018263
CGP	7	0.985119	0.027131	0.032373
SCG	3	0.99281	0.015144	0.016666
SCG	5	0.992972	0.014479	0.018451
SCG	7	0.984103	0.024513	0.029226bb

Figure 7 shows the experimental and predicted values of heat exchanger's oil energy. The best statistical values are obtained with LM10. Obviously, there is a good agreement between predicted and experimentally measured oil energy of the heat exchanger at 12:00 pm. Oil energy reaches its maximum value 0.923 MJ at noon, with a curve clearly decreasing thereafter.

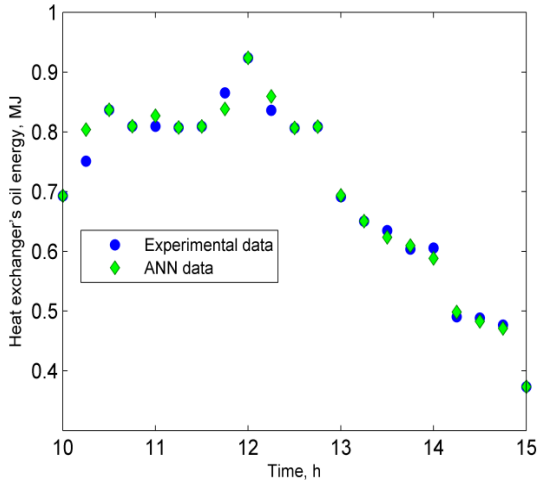

Fig. 7 Comparison of the experimental and predicted values of oil energy of the heat exchanger.

Statistical values of for the heat exchanger's water energy are given in Table 4. Maximum R^2s for train data are respectively 0.999934 & 0.994675, with RMSEs 0.001492 & 0.01426, and MPEs 0.001018 & 0.006791.

Table 4 RMSE and MPE for train data for the heat exchanger's water energy

$Q_{w,H}$				Train data
Algorithms	hl	R_{tr}^2	MPE	RMSE
LM	4	0.994454	0.009821	0.012677
LM	5	0.991638	0.012997	0.01652
LM	6	0.991254	0.012291	0.016176
LM	7	0.995953	0.023663	0.025336
LM	8	0.991926	0.029786	0.033857
LM	9	0.98475	0.015564	0.020089
LM	10	0.999934	0.001018	0.001492
CGP	3	0.957202	0.023067	0.035801
CGP	5	0.975732	0.020185	0.026161
CGP	10	0.956835	0.022621	0.033097
SCG	3	0.976949	0.0186	0.02804
SCG	7	0.971678	0.020666	0.029498
SCG	9	0.967731	0.024027	0.029426

The experimental and predicted values of the heat exchanger's water energy are compared in ''Fig. 8''which portrays their good agreement.

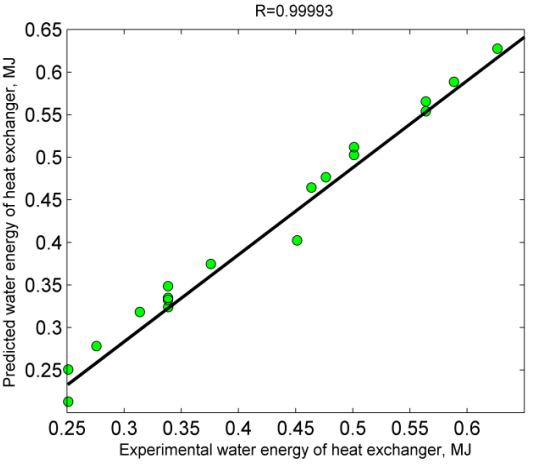

Fig.8 Comparison of the predicted and experimentally determined water energy of heat exchanger.

Table 5 RMSE and MPE for all data for delivered thermal energy to the room

Q_R				All data
Algorithms	hl	R_t^2	MPE	RMSE
LM	4	0.969572	0.036766	0.081187
LM	5	0.970751	0.056953	0.090701
LM	8	0.976451	0.038633	0.074012
LM	9	0.965214	0.063492	0.08305
LM	10	0.997388	0.01367	0.023342
CGP	3	0.96862	0.058544	0.080134
CGP	7	0.923301	0.076019	0.120092
CGP	10	0.937576	0.08168	0.108787
SCG	5	0.944698	0.071261	0.104587
SCG	7	0.964516	0.054975	0.089082
SCG	9	0.971509	0.056457	0.074738

Statistical values of delivered energy to the room are brought into Table 5. Maximum R^2s for train and all data are respectively 0.999916 & 0.997388, with RMSEs 0.005569 & 0.023342, and MPEs 0.004446 & 0.01367. Moreover, maximum RMSEs for train and all data have been ascertained, respectively, 0.077656 & 0.08168.
As seen in Tables 2 to 5, the best R^2 together with the minimum errors are gained for LM algorithm with 10 hidden layers. Delivered thermal energy to the room is represented in ''Fig. 9''. There is less agreement between experimental and ANN data of Q_R, than other operational parameters.

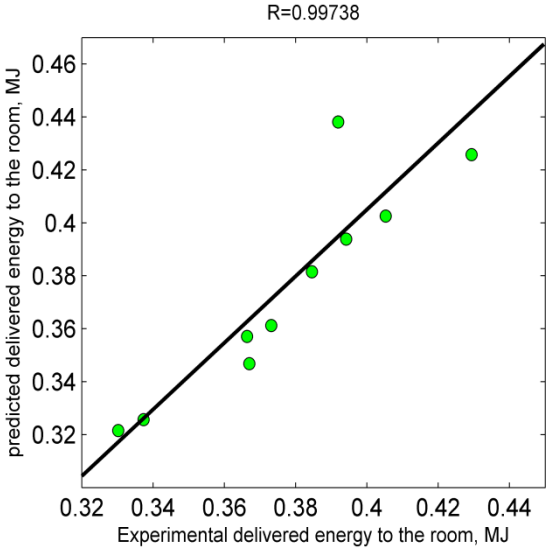

Fig. 9 Predicted and experimental values of delivered energy to the room.

In stage 2, Q_c, Q_R, $Q_{o,H}$ and $Q_{w,H}$ are input parameters, while η_c and η_{Hx} are supposed to be outputs. Table 6 contains statistical values of η_c and used algorithm type for training neural network. Maximum R^2s for train and all data are respectively 0.993323 & 0.986238, with RMSEs 0.005059 & 0.007646, and MPEs 0.002875 & 0.005059. Further, maximum RMSEs for train and all data are, respectively, 0.015241 & 0.015827.

Table 6 RMSE and MPE for all data for collector efficiency

η_c				All data
Algorithms	hl	R_t^2	MPE	RMSE
LM	6	0.986238	0.005059	0.007646
LM	7	0.93826	0.01289	0.015951
LM	8	0.828231	0.016944	0.026034
LM	9	0.943682	0.00948	0.015422
CGP	4	0.925404	0.014373	0.017484
CGP	5	0.921454	0.015827	0.018745
CGP	6	0.923747	0.01575	0.018537
SCG	3	0.950104	0.01097	0.017662
SCG	4	0.915077	0.01479	0.0188
SCG	5	0.95371	0.011344	0.015797

The minimum errors at stage 2 belong to the LM with six hidden layers. Predicted collector efficiency versus experimental collector efficiency is plotted in ''Fig. 10''.

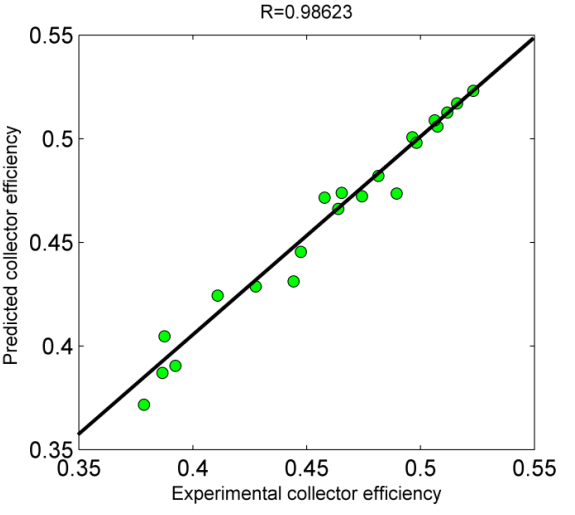

Fig. 10 Predicted collector efficiency versus experimentally determined collector efficiency.

Table 7 contains statistical values of η_H. Maximum R^2s for train and all data are found respectively 0.996766 & 0.99243, with RMSEs 0.005962 & 0.008505, and MPEs 0.004562 & 0.006524. In addition, maximum RMSEs for train and all data would respectively be 0.014023& 0.012899. As seen in Tables 6 & 7, the best R^2 together with minimum errors belong to LM algorithm with 6 hidden layers.

Table 7 RMSE and MPE for all data for the heat exchanger efficiency

η_H				All data
Algorithms	hl	R_t^2	MPE	RMSE
LM	6	0.99243	0.006524	0.008505
LM	7	0.989895	0.006836	0.00867
LM	9	0.979017	0.010731	0.013993
CGP	4	0.949262	0.010342	0.016502
CGP	5	0.925484	0.015138	0.020406
CGP	6	0.942113	0.011134	0.017569
SCG	3	0.95726	0.010115	0.015246
SCG	5	0.934926	0.0156	0.018761
SCG	7	0.936231	0.012899	0.019373

Heat exchanger efficiency was forecasted by the LM, SCG, and CGP algorithms. As illustrated in ''Fig. 11,'' predicted and experimental values of heat exchanger efficiency are well-matched. Heat exchanger and collector efficiencies are inputs of ANN in Stage 3, while the total efficiency of the solar heating system is the target. In this stage, the same algorithms (LM, SCG, and CGP) have been utilized to predict the total efficiency of the system.

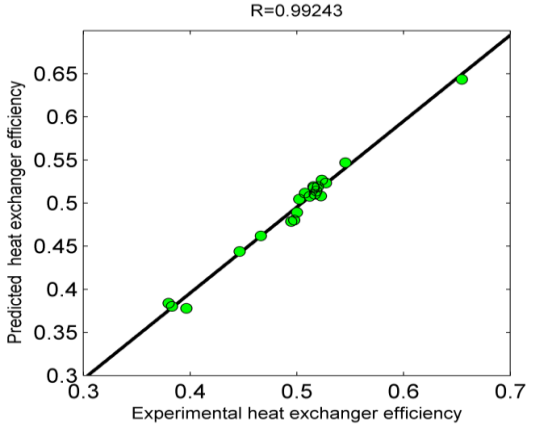

Fig. 11 Predicted and experimental heat exchanger efficiency.

Statistical values for trained and all data are given in ''Tables 8 & 9''. As emboldened, the maximum R^2s for train and all data are 0.999672 & 0.991264, respectively; with RMSEs 0.001189 & 0.0056140, and MPEs 0.0009470 & 0.003066. These values have also been acquired with LM-10. Maximums RMSEs and MPEs would of course be 0.015529 and 0.012885, respectively.

Table 8 RMSE and MPE for train data for the total efficiency of system

η_t				Train data
Algorithms	hl	R_t^2	MPE	RMSE
LM	6	0.990823	0.004827	0.006154
LM	9	0.986137	0.006157	0.007355
LM	10	0.999672	0.000974	0.001189
CGP	4	0.990918	0.004576	0.005777
CGP	6	0.997722	0.002322	0.003116
CGP	10	0.988777	0.0044	0.006866
SCG	4	0.98072	0.005962	0.006792
SCG	8	0.988821	0.004728	0.006167
SCG	9	0.995496	0.003769	0.004396

Table 9 RMSE and MPE for all data for the total efficiency

η_t				All data
Algorithms	hl	R_{tr}^2	MPE	RMSE
LM	6	0.98358	0.005714	00007528
LM	9	0.981516	0.006427	0.00795
LM	10	0.991264	0.003066	0.005614
CGP	4	0.979787	0.005607	0.008271
CGP	6	0.984476	0.00431	0.007366
CGP	10	0.979251	0.005915	0.008333
SCG	4	0.97535	0.007274	0.00886
SCG	8	0.971415	0.007101	0.009887
SCG	9	0.97436	0.007243	0.01006

Figures 12 and 13 show the predicted and experimental total efficiency of the system. The best R^2s of total efficiency for all and the train data are 0.99126 and 0.99967, respectively. Hence, the ANN predicted and experimental efficiencies prove to be well-matched.

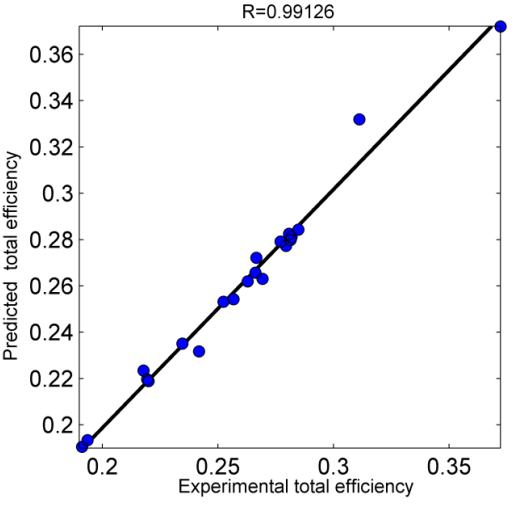

Fig. 12 Predicted and experimental total efficiency for all data.

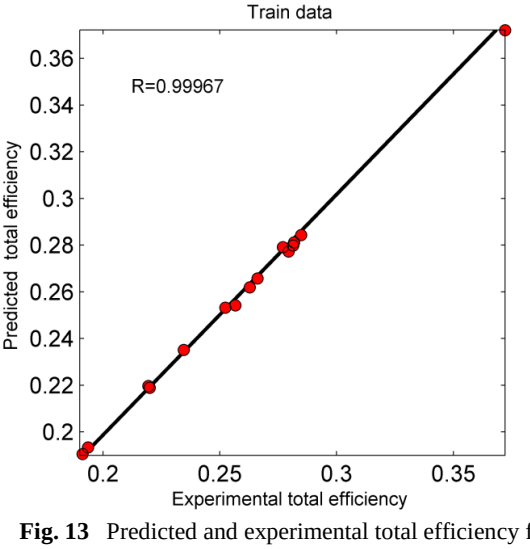

Fig. 13 Predicted and experimental total efficiency for train data.

After three stages, the total efficiency of the system is obtained with high accuracy. In addition, other parameters are derived from stages 1 and 2 with acceptable accuracy. The difference between predicted and experimental efficiency is only 0.00023.

6 CONCLUSION

In this study, first a solar space heating system was set up with PTC. Then, in order to predict the energies of the system components, the collector and heat exchanger efficiencies, and the total efficiency of the solar heating system, a novel multistage ANN was used. LM, SCG, and CGP algorithms were used in the three stages of the ANN. In Stage 1, measured data with experimental tests as inputs were given to multistage ANN. In this Stage,

the designed neural network predicts the useful energy of the collector, energy transferred by the heat exchanger oil, energy obtained by the heat exchanger water, and the energy delivered to the room; with respective maximum RMSE{s} of 0.037041, 0.01423, 0.00444, and 0.01524. These errors are perfectly acceptable for energy systems. In Stage 2, energy values predicted by ANN are used as inputs, and the collector and heat exchanger efficiencies are taken as outputs. In Stage 3, by using the component efficiencies of the system as inputs, the total efficiency is evaluated, with maximum and minimum RMSE{s} of 0.018955 and 0.001189, respectively. The mean predicted and experimental total efficiencies equalled 26%. The best agreement on the predicted parameters with experimental data was given by LM (in Stage 1 with 10, Stage 2 with 6, and Stage 3 with 10 hidden layers). The fastest and most accurate algorithm among the cited algorithms was therefore Levenberg-Marquardt. Since the designed multistage ANN can forecast all parameters of the solar energy system with high accuracy, it can be used to simultaneously predict energy system performance parameters. This ANN could also be employed to validate ANN results with experimental data or analytical solutions.

When there are many target parameters and lots of data for validation, using a multistage ANN can effectively simplify complicated calculations. Fortunately, it can be employed to save time and to predict all parameters simultaneously.

NOMENCLATURE

A	Area (m2)
C_p	Heat capacity ($Jkg^{-1}K^{-1}$)
hl	Hidden layer size
I	Solar radiation (Wm^{-2})
$\dot{m}$	Mass flow rate (kgs^{-1})
Q	Energy
$\dot{Q}$	Power
T_1	The inlet oil temperature of the collector (°C)
T_2	The outlet oil temperature of the collector (°C)
T_3	The inlet oil temperature of the heat exchanger (°C)
T_4	The outlet oil temperature of the heat exchanger (°C)
T_5	The inlet water temperature of the heat exchanger (°C)
T_6	The outlet water temperature of the heat exchanger (°C)
T_7	Temperature of the storage tank water (°C)
T_8	Ambient temperature (°C)
T_9	Room temperature (°C)
T_{10}	The inlet temperature of the radiator(°C)
T_{11}	The outlet temperature of the radiator(°C)
η	Efficiency
a	Ambient
ANN	Artificial neural network
c	Collector
exp	Experimental
H	Heat exchanger
in	Input
o	Oil
out	Output
R	Radiator
st	Storage tank
t	All data
tr	Train
W	Water

REFERENCES

[1] Alamdari, P., Nematollahi, O., and Alemrajabi, A., Solar Energy Potentials in Iran: A Review, Renewable and Sustainable Energy Reviews, Vol. 21, No. 5, 2013, pp. 778-788, http://dx.doi.org/10.1016/j.rser.2012.12.052.

[2] Dehghani sanij, R., Soltani, M. and Raahemifar, K., A New Design of Wind Tower for Passive Ventilation in Buildings to Reduce Energy Consumption in Windy Regions, Renewable and Sustainable Energy Reviews, Vol. 42, Feb., 2015, pp 182–195, http://dx.doi.org/10.1016/j.rser.2014.10.018.

[3] Jovanovic, R. Z., Sretenovic, A. A. and Zivkovic, B. D., Ensemble of Various Neural Networks for Prediction of Heating Energy Consumption, Energy Buildings, Vol. 94, No. 1, 2015, pp. 189-199, https://doi.org/10.1016/j.enbuild.2015.02.052.

[4] Ascione, F., Bianco, N., Stasio, C. D., Mauro, G. M. and Vanoli, G. P., Artificial Neural Networks to Predict Energy Performance and Retrofit Scenarios for Any Member of a Building Category: A Novel Approach, Energy, Vol. 118, No. 1, 2017, pp. 999-1017, http://dx.doi.org/10.1016/j.energy.2016.10.126.

[5] Sholahudin S. and Han, H., Simplified Dynamic Neural Network Model to Predict Heating Load of a Building Using Taguchi Method, Energy, Vol. 115, No. 3, 2016, pp. 1672-1678, https://doi.org/10.1016/j.energy.2016.03.057.

[6] Deb, C., Eang, L. S., Yang, J. and Santamouris, M., Forecasting Diurnal Cooling Energy Load for Institutional Buildings Using Artificial Neural Networks, Energy and Buildings, Vol. 121, No. 1, 2016, pp. 284-297, https://doi.org/10.1016/j.enbuild.2015.12.050.

[7] Argirioua, A. A., Bellas Velidisb, I., Kummert, M. and Andre´c, P., A Neural Network Controller for Hydronic Heating Systems, Neural Networks, Vol. 17, No. 3, 2004, pp. 427-440, doi:10.1016/j.neunet.2003.07.001.

[8] Kalogirou, A. S., Assessment and Simulation Tools for

Sustainable Energy Systems, Springer, London, 2013.

[9] Boukelia, T. E., Arsalan, O. and Mecibah, M. S., ANN-Based Optimization of a Parabolic Trough Solar Thermal Power Plant, Applied Thermal Engineering, Vol. 107, No. 1, 2016, pp. 1210-1218, http://dx.doi.org/10.1016/j.applthermaleng.2016.07.084 .

[10] Hirvonen, J., Rehman, H., Deb, K. and Sirén, K., Neural Network Metamodelling in Multi-Objective Optimization of a High Latitude Solar Community, Solar Energy, Vol. 155, No. 1, 2017, pp. 323–335, http://dx.doi.org/10.1016/j.solener.2017.06.040.

[11] Yaïci, W., Evgueniy, E., Longo, M., Brenna, M. and Federica, F., Artificial Neural Network Modelling for Performance Prediction of Solar Energy System, Proceeding of 4th International Conference on Renewable Energy, Research and Applications, Palermo, Italy, 2015, pp. 22-25.

[12] Liu, Z., Li, H., Zhang, X., Jin, G. and Cheng, K., Novel Method for Measuring the Heat Collection Rate and Heat Loss Coefficient of Water-in-Glass Evacuated Tube Solar Water Heaters Based on Artificial Neural Networks and Support Vector Machine, Energies, Vol. 8, No. 8, 2015, pp. 8814-8834, https://doi.org/10.3390/en8088814.

[13] Elminir, H. K., Areed, F. F. and Elsayed, T. S., Estimation of Solar Radiation Components Incident on Helwan Site using Neural Networks, Solar Energy, Vol. 79, No. 3, 2005, pp. 270–279, doi:10.1016/j.solener.2004.11.006

[14] Mellit, A., Pavan, A. M., A 24-h Forecast of Solar Irradiance using Artificial Neural Network: Application for Performance Prediction of a Grid-Connected PV Plant at Trieste, Italy, Solar Energy, Vol. 84, No. 5, 2010, pp. 807–821, doi:10.1016/j.solener.2010.02.006.

[15] Arat, H., Arslan, O., Optimization of District Heating System Aided by Geothermal Heat Pump: A Novel Multistage with Multilevel ANN Modelling, Applied Thermal Engineering, Vol. 111, No. 1, 2017, pp. 608-623, http://dx.doi.org/10.1016/j.applthermaleng.2016.09.150.

[16] American Society of Heating, R. a. C., International Standard-Solar Energy-Solar Thermal Collector-Test Methods, Geneva, ASHRAE, Iso9806, 2014.

[17] Duffi, J. A., Backman, W. A., Solar Engineering of Thermal Processes, 3nd ed, Wiley, Wisconsin, Madison, 2006, Chaps. 3, Vol. 6.